Int. J. Electrochem. Sci., 11 **(2016)** 5080 – 5089, doi: 10.20964/2016.06.75

International Journal of
ELECTROCHEMICAL
SCIENCE
www.electrochemsci.org

Assembly of Mn_3O_4/carbon Black Composite and Its Supercapacitor Application

Xugang Ren[1], *Junwei An*[2], *Shaohui Yan*[1,*], *Lizhen Gao*[1], *Shengming Xu*[2,*], *Xiaomin Wang*[3], *Guoqiang Wei*[3]

[1] College of Environmental Science and Engineering, Taiyuan University of Technology, Taiyuan, 030024, China
[2] Institute of Nuclear and New Energy Technology, Tsinghua University, Beijing 100084, China
[3] Laboratory of Green Energy Materials and Storage Systems, Taiyuan University of Technology, Taiyuan, 030024, China
[*]E-mail: shyan@buaa.edu.cn

Received: 11 March 2016 / *Accepted:* 18 April 2016 / *Published:* 4 May 2016

In this article, Mn_3O_4 nanoparticles are prepared directly on a commercial high conductive carbon black (CB) to form a Mn_3O_4/carbon black composite (Mn_3O_4/CB) by a chemical synthesis method. The TEM results indicate that the microstructure of the Mn_3O_4 nanoparticles in the Mn_3O_4/CB composite is in good order, and they are distributed on the surface of carbon black uniformly. The electrochemical properties revealed from the rectangularity of the cyclic-voltammogram loops of the composite electrode are satisfactory. These results indicate the almost-ideal capacitive behavior of the Mn_3O_4/CB composite. The electrochemical tests indicate that the specific capacitance of the Mn_3O_4/CB composites reaches 720 F/g at the current density of 0.1 A/g in 2 M Na_2SO_4 solution, which is approximately 4.36 times than that of the pristine Mn_3O_4 (165 F/g). The Mn_3O_4/CB composite electrode shows excellent capacity retention (91.6%) after 5000 cycles at the current density of 30 A/g.

Keywords: supercapacitor; Mn_3O_4; carbon black; electrode materials

1. INTRODUCTION

The ever-worsening energy and environment issues call for advanced energy-storage devices. Supercapacitors and lithium-ion batteries are considered to be the two important energy-storage devices. Compared with lithium-ion batteries, supercapacitors possess a much- longer cycle life, much-higher power densities, and much-shorter charge/discharge times, but relatively lower energy densities [1,2]. In terms of the electrode materials for supercapacitors, transition metal oxides have drawn

extensive research attention, such as MnO_2, Fe_2O_3, IrO_2, and RuO_2 etc. [3-7], because they provide double layer capacitance and pseudocapacitive, simultaneously [8-13]. Manganese oxide (MnO_x) has drawn more and more attention due to its low price and environment friendly features [6,14,15]. It was reported that the specific capacitance of α-MnO_2 prepared by an anodic-deposition method reaches 320 F/g in 0.1 M Na_2SO_4 solution at a scan rate of 25 mV/s [16]. In order to improve the specific capacitance of MnO_2, many people try to mix it with a variety of carbon materials [17-22].

In recent years, Mn_3O_4 is also considered as supercapacitor electrode material, due to its stable morphology and controllable microstructure [23]. Compared with MnO_2, Mn_3O_4 has much superior, such as uniform structure, stable performance and easily obtain pristine phase Mn_3O_4 [24]. Therefore, Mn_3O_4 has a wide range of applications in catalysis, ion exchange, molecular adsorption and electrochemical materials [25-30]. For improving the specific capacitance of Mn_3O_4, many researchers have investigated Mn_3O_4 composite electrode materials with graphene nanosheets. The capacitive properties of Mn_3O_4 nanoparticles anchored graphene nanocomposite studied in the presence of 1 M Na_2SO_4 exhibited high specific capacitance of 312 F/g [24]. MWCNT/Mn_3O_4 composite obtained by anchoring Mn_3O_4 nanoparticles to multiwall carbon nanotubes reaches a highest specific capacitance of 441 F/g at 2 mV/s scan rate [31].

Compared with graphene, carbon black (CB) used in industrial production has merits of low price and environment friendly [32]. Moreover, it has been widely used in supercapacitor electrode and lithium-ion batteries as a conductive additive [33, 34]. In this work, a series of Mn_3O_4/carbon black composite (Mn_3O_4/CB) is synthesized by a chemical synthesis method directly on the surface of carbon black. The preparation process is illustrated in Figure 1, it can be found that the Mn_3O_4 nanoparticles are arranged on the surface of carbon black uniformly. The electrochemical performance of the Mn_3O_4/CB composite is measured by galvanostatic charge-discharge. The results show that the Mn_3O_4/CB composite reaches a specific capacitance of 720 F/g at a current density of 0.1 A/g in 2 M Na_2SO_4 solution. Furthermore, only a little decay of less than 8.4% after the 5000th cycle implies its extraordinary cycling stability.

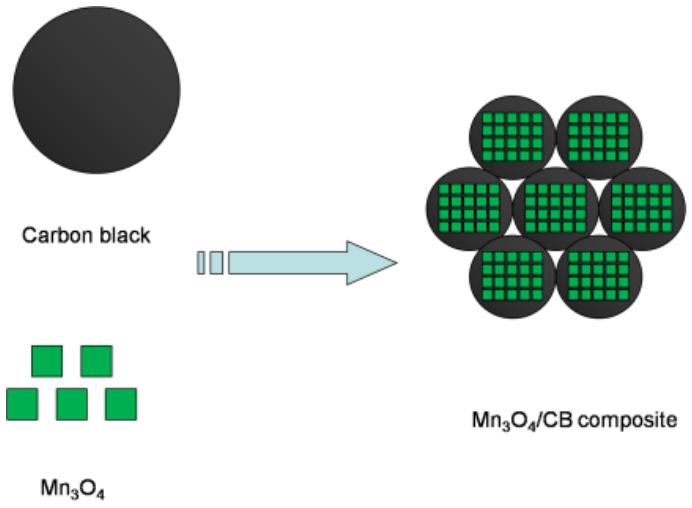

Figure 1. Schematic illustration of the preparation of Mn_3O_4 /CB composite.

2. EXPERIMENTAL SECTION

Fabrication of the composite and pristine Mn_3O_4: The synthesis process is illustrated in Figure 1. Firstly, 3.5 mmol of manganese (Ⅱ) acetate (0.875 g), 12.5 mmol of oleylamine (3.35 g), and 2.5 mmol of oleic acid (0.71 g) are dissolved in 75 ml of xylene in air atmosphere. Then, 0.01 g of commercial carbon black is added into the solution, stirred and sonicated for 30 min respectively. After that, the mixture is heated to 40 ℃ and stirred for 1h, followed by heated it to 90℃slowly (kept for 15 minutes per 10 ℃), 15 minutes later, 5 ml distilled water is injected into the solution under vigorous stirring, and the resulting solution is aged at 90 ℃ for 2 h. After the temperature of the reaction system is cooled to room temperature, 70 ml of ethanol is decanted into the reactor. The mixture is aged for 1h, the resultant sample filtered, washed with ethanol for several times, and finally dried in an oven at 80 ℃ for 10 h. The sample labeled as Mn_3O_4/CB-0.01. In the same process of preparation, Mn_3O_4/CB-0.03 and Mn_3O_4/CB-0.05 are obtained by change the amount of carbon black to 0.03 g and 0.05 g, respectively. Pristine Mn_3O_4 is obtained without the addition of carbon black [35].

Materials Characterization: Transmission electron microscope (TEM) and X-ray diffraction (XRD) equipment are used to characterize the texture, morphology and chemical structure of carbon black, pristine Mn3O4 and Mn_3O_4/CB-0.03. The TEM measurements are conducted on a JEM 1200EX microscope at 80kV and Tecnai G2 F20 S-TWIN microscope at 200kV. XRD spectra of Mn_3O_4/CB composite and its components are recorded on a Rigaku Dmax 2400 X-ray diffractometry.

Electrochemical test: The electrochemical tests are carried out in a three–electrode configuration with a Pt plate counter electrode and a Ag/AgCl reference electrode in 2 M Na_2SO_4 aqueous solution with pH=10, which is adjusted by KOH solution. The working electrode is prepared by dispersing 20 mg Mn_3O_4/CB composite into 20 ml ethanol (5% water) containing 30 μL Nafion solution and sonicat for 15 minutes, then dropping it onto the glassy carbon electrode with a diameter of 5mm and drying at room temperature for 4 h before electrochemical test. The electrochemical performance of the electrode materials is evaluated by cyclic voltammetry (CV) and galvanostatic charge-discharge and alternating current impedance techniques using a CHI 760e electrochemical workstation (Shanghai, China).

3. RESULTS AND DISCUSSION

Figures 2a and b display the TEM images of the pristine Mn_3O_4 and carbon black, respectively. According to these figures, the Mn_3O_4 nanoplates are grown on the surface of carbon black successfully. The TEM image of the Mn_3O_4/CB composite shown in Figure 2c consists of cubic Mn_3O_4 arrays and carbon black, and the length of side of tetragonal Mn_3O_4 is around 10nm.

Figure 3a shows the XRD pattern of carbon black, Mn_3O_4/CB-0.03 and pristine Mn_3O_4. As shown in Figure 3a, there are four obvious diffraction peaks at 2θ around 18.294°, 36.486°, 44.574° and 60.223°.

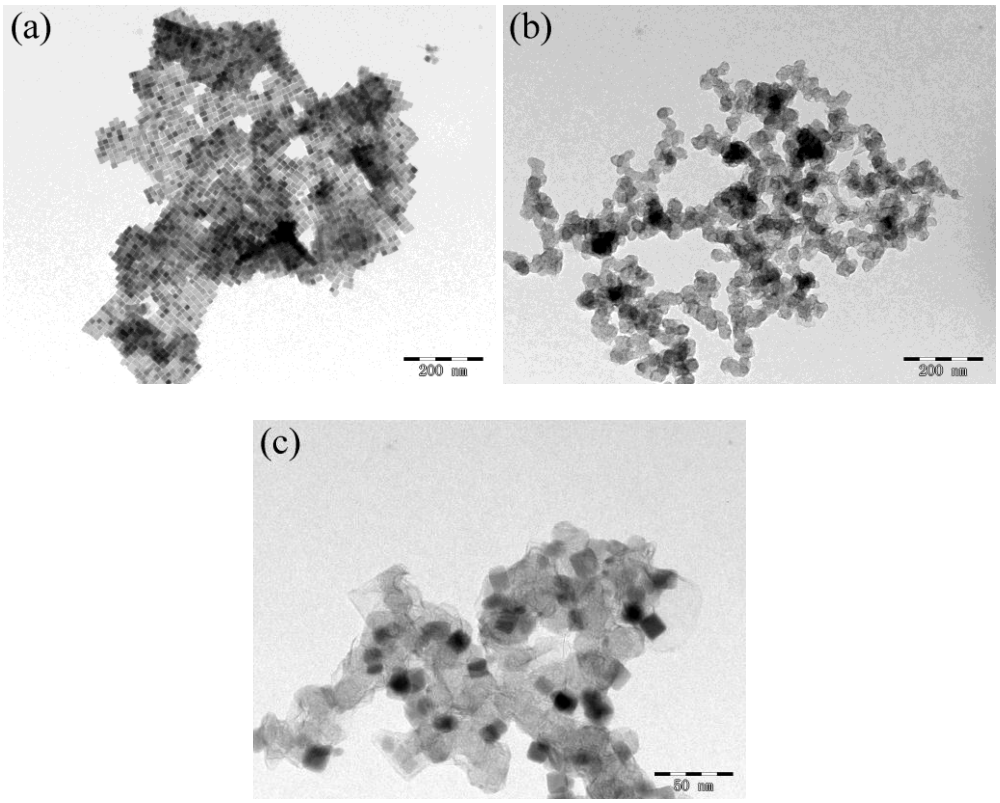

Figure 2. TEM images of pristine Mn_3O_4 (a), carbon black (b), and the Mn_3O_4/CB composites (c).

These four peaks can be indexed to tetragonal Mn_3O_4 structure (JCPDS card no. 24-0734) [4]. Meanwhile, there are two obvious diffraction peaks of carbon black at 2θ around 26.2° and 44.3°, which are related to hexagonal carbon (JCPDS No. 75-1621). The diffraction peak located at 26.3° of Mn_3O_4/CB composite corresponds with hexagonal carbon, which proved the existence of carbon black in Mn_3O_4/CB composite. Moreover, the XRD pattern of the Mn_3O_4/CB composite also displays the diffraction peaks of the Mn_3O_4, these results proved again that the Mn_3O_4/CB composite is successfully prepared by the chemical synthesis method.

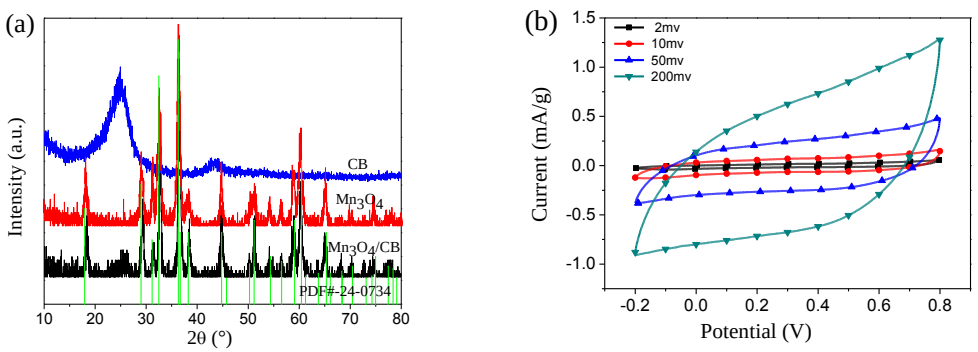

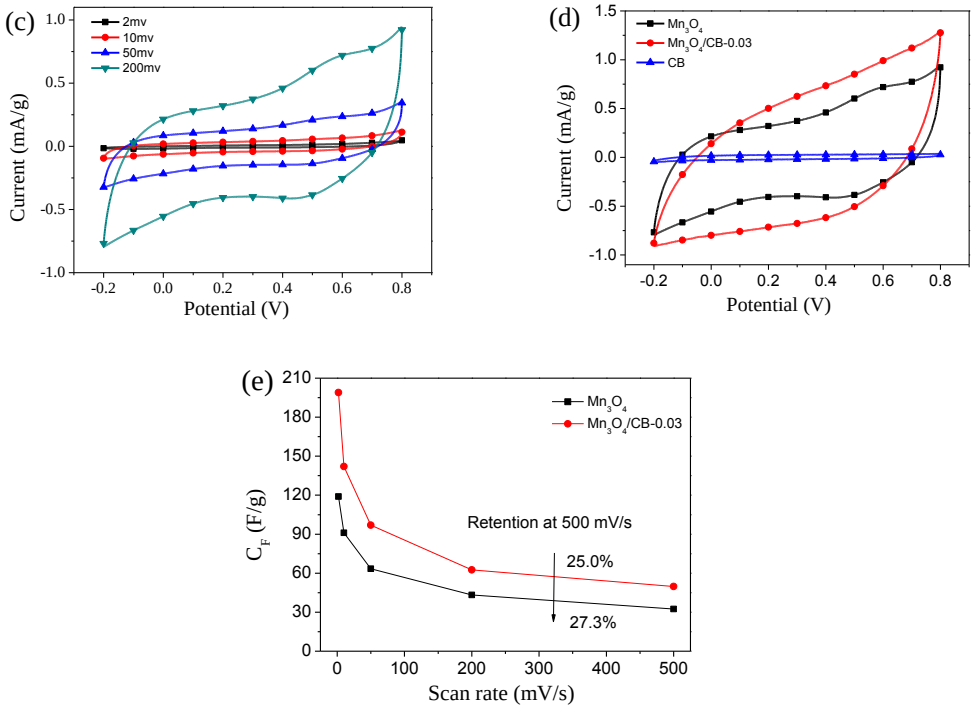

Figure 3. (a) The XRD pattern of the Mn_3O_4/CB-0.03 composite, pristine Mn_3O_4 and conductive carbon black. (b) CV curves of the Mn_3O_4/CB-0.03 composite at different scan rates. (c) CV curves of the pristine Mn_3O_4 at different scan rates. (d) CV curves of the Mn_3O_4/CB composite, Mn_3O_4 and carbon black at 200mV/s scan rate. (e) C_F versus sweep rates for Mn_3O_4/CB-0.03 and pristine Mn_3O_4

Various scan rates of 2, 10, 50, and 200 mV/s are respectively applied in CV measurement to study the capacitive behaviors of Mn_3O_4/CB-0.03 and pristine Mn_3O_4 electrodes between -0.2-0.8 V. The corresponding CV curves are displayed in Figure 3b and Figure 3c, respectively. The profiles of CV curves present roughly rectangular mirror images without obvious redox peaks in Figure 3b, indicating the Mn_3O_4/CB-0.03 has an ideal capacitive behaviors caused by the introduction of conductive carbon black. With the increase of scan rates, the CV curves gradually deviate from rectangular shapes and the area of CVs enlarge. Compared with Mn_3O_4/CB-0.03, the CV curves of the pristine Mn_3O_4 (Figure 3c) have a slight bulge, due to the Faradaic redox reaction [36,37]. Moreover, the CV curves of the Mn_3O_4/CB-0.03 electrode at the scan rate of 200 mV/s have a much larger integrated area compared to that of the pristine Mn_3O_4 electrode or carbon black (Figure 3d), indicating the higher specific capacitance is achieved in the Mn_3O_4/CB electrodes. This phenomenon suggests that the addition of carbon black with high conductivity can promote the specific capacitance of the Mn_3O_4/CB composite, significantly. The capacitive plots for CV curves at different scan rates are shown in Figure 3e. The Mn_3O_4/CB-0.03 exhibits the highest capacitive value for all range of sweep rates. The initial CF at 3 mV/s is remarkably decreased both for Mn_3O_4/CB-0.03 and pristine Mn_3O_4. With the increase of sweep rates, the capacitive value decreased gradually and the retention of CF at sweep rate of 500 mV/s for Mn_3O_4/CB-0.03 and pristine Mn_3O_4 are 25.0% and 27.3%. With the increase of sweep rates, the CF of Mn_3O_4/CB-0.03 decreased due to the delay of potential during

reversing the potential sweep, which is related to a kinetically slow process involved during charging/discharging the pseudocapacitance [38,39].

Figure 4a and b indicate the galvanostatic charge-discharge behaviors of Mn_3O_4/CB-0.03 and pristine Mn_3O_4 electrodes at current densities of 0.1-10 A/g, respectively. It can be seen from Figure 4a and b, the charge-discharge curves both exhibited a symmetrical triangle at high current densities, indicating a good electrochemical capacitive characteristic and superior reversible redox reaction [36,40]. However, the curves are bent generally with the decrease of the current, because of the redox reactions caused by the Faradic pseudocapacitance [41,42]. In the large currents, the electrolyte ions with fast speed hardly enter the interior of material to carry on electrochemical reaction, resulting in the bending is not obvious [21]. It is found that, the specific capacitance of electrode increases with the decrease of the current density. The possible reason is the movement rate of ions become slowly as the current decreases, causing the electrode reaction takes place on the electrode surface and in the bulk phase at the same time [43,44]. The rate capability of Mn_3O_4/CB-0.03 increases to 720 F/g at 0.1A/g from 300 F/g at 0.3A/g while the rate performance of pristine Mn_3O_4 seems to have no obvious change. Which indicate the availability of microstructure of carbon black is improved obviously as the decreases of the current density. The specific capacitance of Mn_3O_4/CB-0.03 is higher than that of the Mn_3O_4 composites reported in literatures [45,46]. The possible reason of excellent specific capacitances of the Mn3O4/CB-0.03 is that carbon black enhances the electronic transportation.

Figure 4c and d compare the charge-discharge curves of the Mn_3O_4/CB-0.03, pristine Mn_3O_4 and carbon black at the current density of 0.1 A/g and 1 A/g, respectively. It can be seen clearly that the specific capacitances of the Mn_3O_4/CB-0.03 are higher than that of pristine Mn_3O_4 under all current densities, indicating again that the introduction of carbon black can greatly improve the specific capacitance of pristine Mn_3O_4. The specific capacitance of Mn_3O_4/CB-0.03 is measured to be 720 F/g in 2 M Na_2SO_4 electrolyte at a current density of 0.1 A/g. The possible reason of excellent specific capacitances of the Mn_3O_4/CB-0.03 is that carbon black enhances the electronic transportation.

The coulombic efficiency of Mn_3O_4/CB-0.03 and pristine Mn_3O_4 calculated from Figure 4c, d reaches 1.46, 0.95 (0.1A/g) and 1.06, 0.95 (1 A/g). We can find that the coulombic efficiency of Mn_3O_4/CB-0.03 are larger than pristine Mn_3O_4 both at current densities of 0.1 A/g and 1 A/g. we also can calculated from Figure 4c that the energy density and power density of Mn_3O_4/CB-0.03 reaches 100 wh/kg, 50.5 w/kg at a current densities of 0.1 A/g and pristine Mn_3O_4 reaches 22.9 wh/kg, 53.2 w/kg. The energy density of Mn_3O_4/CB-0.03 is larger than pristine Mn_3O_4 and other reported electrode materials [47, 48]. However, the power density of Mn_3O_4/CB-0.03 is very close to the pristine Mn_3O_4, due to redox reactions caused by Faradic psedocapacitance**.**

Figure 4e compares the charge-discharge curves of the Mn_3O_4/CB-0.01, Mn_3O_4/CB-0.03, Mn_3O_4/CB-0.05 and pristine Mn_3O_4 at a current density of 3 A/g. The specific capacitances of the Mn_3O_4/CB-0.01, Mn_3O_4/CB-0.03, Mn_3O_4/CB-0.05 and pristine Mn_3O_4 calculated from Figure 4a-e at different current densities are list in Table 1. According to Table 1, the specific capacitance of the Mn_3O_4/CB-0.03 is the greatest among the Mn_3O_4/CB composites, indicating that the synthesizing ratio between manganese (Ⅱ) acetate and carbon black for the Mn_3O_4/CB-0.03 is the most appropriate proportion.

Cycle life tests over 5000 cycles for both hybrid and pristine Mn_3O_4 arrays are carried out at the current density of 30 A/g. As shown in Figure 4f, the capacitance loss for the Mn_3O_4/CB-0.03 after 5000 cycles is only 8.4 %, while the capacitance loss for the pristine Mn_3O_4 is about 36.4%. The cycle stability of the Mn3O4/CB-0.03 is better than that of the porous Mn3O4 (78% is remained after 5000 cycles at a current density of 5 A/g) reported in literature [49]. This result implies the hybrid exhibits a good long-term electrochemical stability.

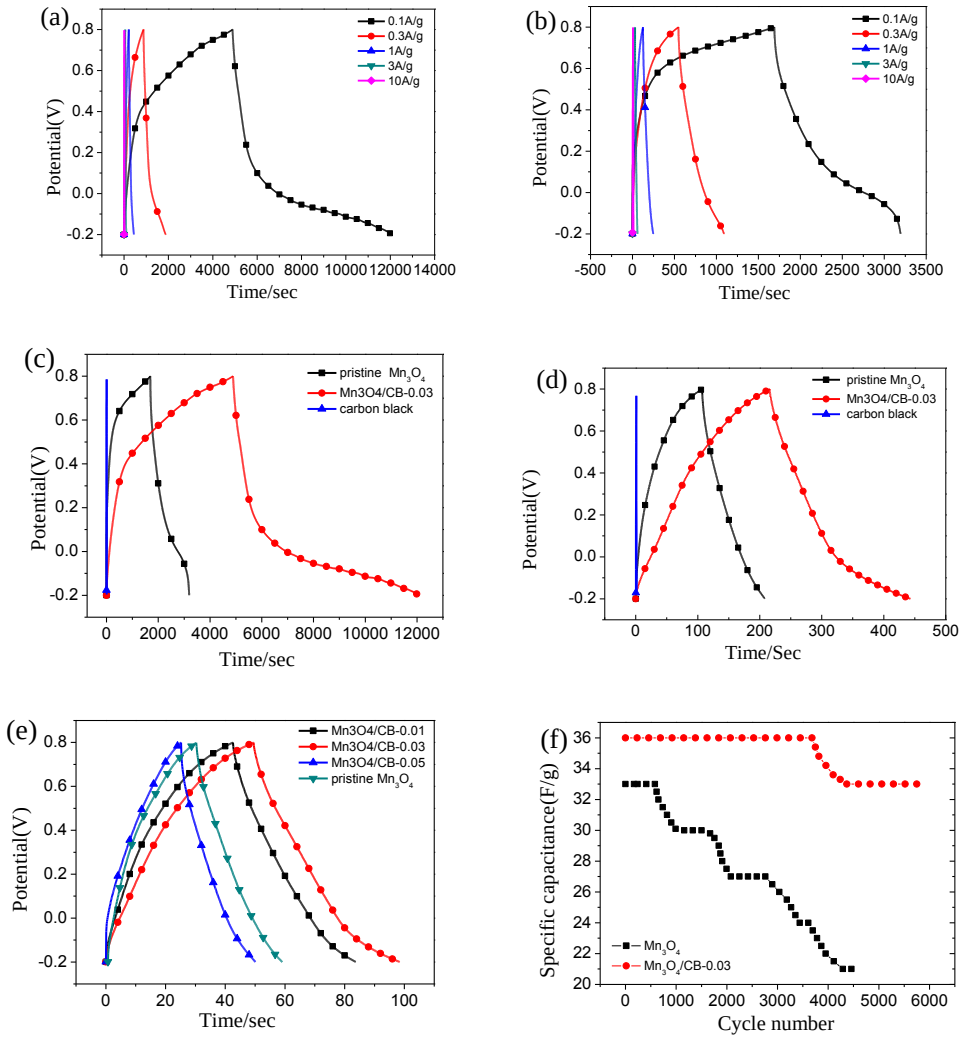

Figure 4. Charge/discharge curves of the Mn_3O_4/CB-0.03 (a) and pristine Mn_3O_4 (b) at different current densities. Charge/discharge curves for Mn_3O_4/CB-0.03, pristine Mn_3O_4 and carbon black at current density of 0.1A/g (c) and 1A/g (d). (e) Charge/discharge curves of the Mn_3O_4/CB-0.01, Mn_3O_4/CB-0.03, Mn_3O_4/CB-0.05 and pristine Mn_3O_4 at 3A/g current density. (f) Cycling stability test for the Mn_3O_4/CB-0.03 and pristine Mn_3O_4 after 5000 cycles at current density of 30A/g.

As one of the fundamental measuring methods, the electrochemical impedance spectroscopy (EIS) is applied to further investigate the electrochemical interfacial behavior. The EIS spectra of Mn_3O_4/CB-0.03 and pristine Mn_3O_4 are shown in Figure 5a. As shown in Figure 5a, the EIS spectra

consist of the contact resistance (R_e) of the active material/current collector interface and the charge transfer resistance (R_{ct}).

Table 1. Specific capacitance of the Mn_3O_4/CB-0.01, Mn_3O_4/CB-0.03, Mn_3O_4/CB-0.05 and pristine Mn_3O_4 calculated from Figure 4a-e at different current densities

	10（A/g）	3（A/g）	1（A/g）	0.3（A/g）	0.1 (A/g）
Mn_3O_4	55	84	120	150	165
Mn_3O_4/CB-0.01	90	110	200	285	670
Mn_3O_4/CB-0.03	110	150	220	300	720
Mn_3O_4/CB-0.05	60	90	134	255	425

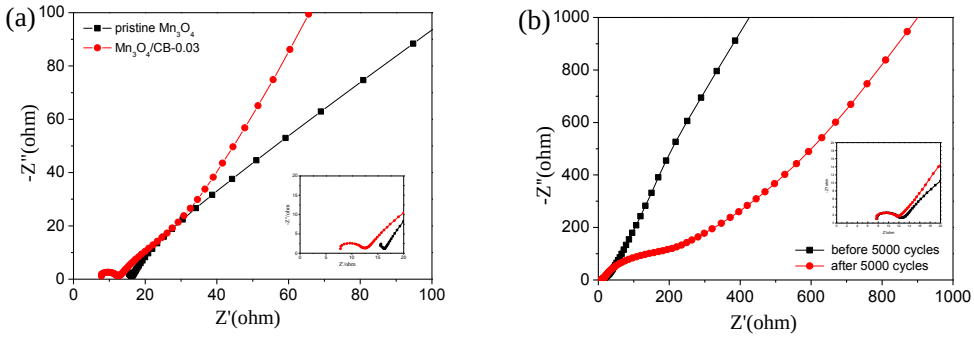

Figure 5. (a) Nyquist plots for the Mn_3O_4/CB-0.03 and pristine Mn_3O_4. (b) Nyquist plots for the Mn_3O_4/CB-0.03 before and after 5000 cycles at current density of 30 A/g. The inset is an enlargement of the high-frequency region of the Nyquist plots.

At low frequency region, the electrode is controlled by diffusion processes. The steep slope revealed in Figure 5a indicates that the electrode exhibits excellent capacitance property [50,51]. R_e of the Mn_3O_4/CB-0.03 and the pristine Mn_3O_4 are measured to be 7.6 and 9.9Ω respectively, and R_{ct} of the Mn_3O_4/CB-0.03 and the pristine Mn_3O_4 are measured to be 5.1 and 7.1 Ω. Therefore, the conductivity of hybrid increased significantly makes the charge transfer impedance reduced significantly due to the introduction of conductive carbon black. The EIS curves exhibit a steep slope at the low frequency region attributes to the non-Faradaic charge storage mechanism. Moreover, the EIS of the Mn_3O_4/CB-0.03 before and after 5000 cycles are performed; the corresponding results are shown in Figure 5b. According to Figure 5b, semicircle of high frequency region of Mn_3O_4/CB-0.03 almost coincides with that of after 5000 cycles, suggesting its R_e and R_{ct} almost unchanged. Furthermore, the slope of the line at the low frequency region becomes smooth, suggesting the Warburg resistance (Z_w), the response of the frequency dependence of ion transport in the electrolyte,

becomes increase. This phenomenon indicates that its capacitor characteristics are decreased after 5000 cycles. This is caused by passivation of a small amount of Mn_3O_4.

4. CONCLUSIONS

In summary, a kind of novel Mn_3O_4/CB composite with high specific capacitance is fabricated by a facile strategy. The TEM tests exhibit the cubic Mn_3O_4 array directly on the surface of carbon black uniformly. In CV tests, Mn_3O_4/CB displayed good capacitive response; the profiles of CV curves present roughly rectangular mirror images without obvious redox peaks. High capacitance (e.g., 720F/g at 0.1 A/g current density in 2 M Na_2SO_4 solution), and excellent cycling stability (8.4% loss over 5000 cycles at a high current density of 30A/g) are achieved in the as-fabricated Mn_3O_4/CB electrode. And the hybrid can take full advantages of conductive carbon black, improves its conductivity and other electrochemical properties. Therefore, the Mn_3O_4/CB nanoplates array has a broad scope in electrochemical supercapacitors.

ACKNOWLEDGEMENTS
This work is supported by the Scientific and Technological Innovation Programs of Higher Education Institutions in Shanxi (STIP, 2014113) and Natural Science Foundation of Shanxi (2014011017-2).

References

1. C. Wang, F. Li, H. Qu, Y. Wang, X. Yi, Y. Qiu, Z. Zou, Y. Luo and B. Yu, *Electrochim. Acta*, 158 (2015) 35.
2. Y. H. Lin, T. Y. Wei, H. C. Chien and S. Y. Lu, *Adv. Energy Mater.*, 1 (2011) 901.
3. M. Winter and R. J. Brodd, *Chem. Rev.*, 104 (2004) 4245.
4. J. Duan, S. Chen, S. Dai and S. Z. Qiao, *Adv. Funct. Mater.*, 24 (2014) 2072.
5. L. Lian, J. Yang, P. Xiong, W. Zhang and M. Wei, *RSC Adv.*, 4 (2014) 40753.
6. N. B. Trung, T. V. Tam, D. K. Dang, K. F. Babu, E. J. Kim, J. Kim and W. M. Choi, *Chem. Eng. J.*, 264 (2015) 603.
7. Y. Du, X. Zhao, Z. Huang, Y. Li and Q. Zhang, *RSC Adv.*, 4 (2014) 39087.
8. R. K. Selvan, I. Perelshtein, N. Perkas and A. Gedanken, *J. Phys. Chem. C*, 112 (2008) 1825.
9. W. W. Zeng, K. L. Huang, Y. P. Yang, S. Q. Liu and R. S. Liu, *Acta Phys. Chim. Sin.*, 24 (2008) 263.
10. M. Toupin, T. Brousse and D. Bélanger, *Chem. Mater.*, 16 (2004) 3184.
11. M. S. Wu and H. H. Hsieh, *Electrochim. Acta*, 53 (2008) 3427.
12. B. H. Zhang and N. Zhang, *Acta Phys. Chim. Sin.*, 19 (2003) 286.
13. A. A. F. Grupioni, E. Arashiro and T. A. F. Lassali, *Electrochim. Acta*, 48 (2002) 407.
14. O. Bricker, *Am. Mineral.*, 50 (1965) 1296.
15. M. M. Thackeray, *Prog. Solid State Ch.*, 25 (1997) 1.
16. C. C. Hu and T. W. Tsou, *Electrochem. Commun.*, 4 (2002) 105.
17. X. P. Dong, W. H. Shen, J. L. Gu, L. M. Xiong, Y. F. Zhu, Z. Li and J. L. Shi, *J. Phys. Chem. B*, 110 (2006) 6015.
18. A. E. Fischer, M. P. Saunders, K. A. Pettigrew, D. R. Rolison and J. W. Long, *J. Electrochem. Soc.*, 155 (2008) A246.
19. G. R. Li, Z. P. Feng, Y. N. Ou, D. C. Wu, R. W. Fu and Y. X. Tong, *Langmuir*, 26 (2010) 2209.
20. Q. Cheng, J. Tang, J. Ma, H. Zhang, N. Shinya and L. C. Qin, *Carbon*, 49 (2011) 2917.

21. Q. Li, X. N. Hu, Q. Yang, Z. Yan, L. P. Kang, Z. B. Lei, Z. P. Yang and Z. H. Liu, *Electrochim. Acta* 119 (2014) 184.
22. V. H. Nguyen, V. C. Tran, D. Kharismadewi and J. J. Shim, *Mater. Lett.*, 147 (2015) 123.
23. X. H. Lv, W. Lv, W. Wei, X. Y. Zheng, C. Zhang, L. J. Zhi and Q. H. Yang, *Chem. Commun.*, 51 (2015) 3911.
24. B. G. S. Raj, R. N. R. Ramprasad, A. M. Asiri, J. J. Wu and S. Anandan, *Electrochim. Acta*, 156 (2015) 127.
25. F. Yang, M. Zhao, Q. Sun and Y. Qiao, *RSC Adv.*, 5 (2015) 9843.
26. Y. Dai, K. Wang and J. Xie, *Appl. Phys. Lett.*, 90 (2007) 104102.
27. S. Nagamuthu, S. Vijayakumar and G. Muralidharan, *Dalton Trans.*, 43 (2014) 17528.
28. Y. Dan, H. Lin, X. Liu, H. Lu, J. Zhao, Z. Shi, Y. Guo, *Electrochim. Acta*, 83 (2012) 175.
29. Y. Liu, W. Wang, Y. Wang, Y. Ying, L. Sun and X. Peng, *RSC Adv.*, 4 (2014) 16374.
30. M. O. Danilov and A. V. Melezhyk, *J. Power Sources*, 163 (2006) 376.
31. M. Chanchal, G. Debasis, A. Teresa, S. A. Kumar and P. Tarasankar, *New J. Chem.*, 39 (2015) 8373.
32. G. Yu, L. Hu, M. Vosgueritchian, H. Wang, X. Xie, J. R. McDonough, X. Cui, Y. Cui and Z. Bao, *Nano Lett.*, 11 (2011) 2905.
33. Z. Yu, B. Duong, D. Abbitt and J. Thomas, *Adv. Mater.*, 25 (2013) 3302.
34. J. Y. Luo and Y. Y. Xia, *Adv. Funct. Mater.*, 17 (2007) 3877.
35. T. Yu, J. Moon, J. Park, Y. I. Park, H. B. Na, B. H. Kim, I. C. Song, W. K. Moon and T. Hyeon, *Chem. Mater.*, 21 (2009) 2272.
36. M. S. Wu , Z. S. Guo, J. J. Jow, *J. Phys. Chem. C*, 114 (2010) 21861.
37. Y. Y. Gao, S. L. Chen, D. X. Cao, G. L. Wang and J. L. Yin, *J. Power Sources*, 195 (2010) 1757.
38. C. M. Chen, Q. Z., M. Guo, C. H. Huang, Y. G. Yang and M. Z. Wang, *Carbon*, 50 (2012) 3572.
39. E. Frackowiak and F. Beguin, *Carbon*, 39 (2001) 937.
40. J. W. Liu, J. Essner and J. Li, *Chem. Mater.*, 22 (2010) 5022.
41. C. Liu, F. Li , L. P. Ma and H. M. Cheng , *Adv. Mater.*, 22 (2010) E28.
42. R. Kötz and M. Carlen, *Electrochim. Acta*, 45 (2000) 2483.
43. J. H. Kim, K. Zhu , Y. F. Yan , C. L. Perkins and A. Frank, *Nano Lett.*,10 (2010) 4099.
44. C. J. Yu , C. Masarapu , J. P. Rong , B. Q. Wei and H. Q. Jiang, *Adv. Mater.*, 21 (2009) 4793.
45. G. R. Xu, J. J Shi, W.H. Dong, Y. Wen, X. P. Min and A. P. Tang, *J. Alloy. Compd.*, 630 (2015) 266.
46. R. T. Dong, Q. L. Ye, L. L. Kuang, X. Lu, Y. Zhang, X. Zhang, G. J. Tan, Y. X. Wen and F. Wang, *ACS Appl. Mater. Inter.*, 5 (2013) 9508.
47. L. Z. Yu, Akhtar, M. Shaheer and Y. O. Bong, *J. Alloy. Compd.*, 653 (2015) 212.
48. C. F. Liu, H. Q. Song, C. K. Zhang, Y. G. Liu, C. P. Zhang, X. H. Nan and G. Z. Cao, *Nano Res.*, 8 (2015) 3372.
49. Y. Q. Qiao, Q. J. Sun, J. Y. Xia, H. Y. Cui, Y. F. Tang and X. H. Wang, *J. Alloy. Compd.*, 660 (2016) 416.
50. T. C. Girija and M. V. Sangaranarayanan, *J. Power Sources*, 156 (2006) 705.
51. W. C. Chen and T. C. Wen, *J. Power Sources*, 117 (2003) 273.